This article has been accepted for publication in IEEE Transactions on Dielectrics and Electrical Insulation. This is the author's version which has not been fully edited and content may change prior to final publication. Citation information: DOI 10.1109/TDEI.2025.3635100

Two-step Broadband Equivalent Circuit Modeling Method for Power Transformer Winding Based on Frequency Response Analysis and Bayesian Optimization

Yu Chen, Jiangnan Liu, Yuxuan Ding, Yaping Du, Binghao Li, Chenguo Yao, *Member, IEEE*, Zhongyong Zhao, *Member, IEEE*

***Abstract*— Frequency response analysis (FRA) is a well-established technique to detect transformer winding deformation faults. Its diagnostic application is based on the principle that a transformer winding can be represented by an equivalent circuit consisting of resistors, inductors, and capacitors. However, rapidly obtaining an accurate and physically meaningful broadband equivalent circuit model for windings remains challenging, limiting both the understanding of fault mechanisms and the generation of data for data-driven fault diagnosis methods. To address these difficulties, this study proposes a two-step broadband equivalent circuit modeling method for the transformer winding based on FRA and Bayesian optimization (BO), considering long-distance mutual inductances and capacitances. The proposed method is validated in a specially designed 10 kV power transformer. Subsequently, two kinds of winding deformation faults, including inter-disk short circuits (IDSCs) and disk space variations (DSVs), are simulated on the basis of the built model and compared with the experimental FRA data. The validation results confirm the accuracy and effectiveness of the proposed method in the construction of the equivalent winding circuit.**

***Index Terms*— Winding modeling, broadband equivalent circuit, frequency response analysis, Bayesian optimization.**

This work was supported in part by the China Southern Power Grid under Grant No. ZBKJXM20232293, in part by the Fundamental Research Funds for the Central Universities under Grant SWU-KT22027, and in part by the National Natural Science Foundation of China under Grant 51807166 (*Corresponding author: Zhongyong Zhao and Yuxuan Ding*).

Yu Chen, Yuxuan Ding, and Yaping Du are with the Department of Building Environment and Energy Engineering, The Hong Kong Polytechnic University, Hong Kong, China (e-mail: yu2000.chen@connect.polyu.hk, yuxuanz.ding@polyu.edu.hk, yaping.du@polyu.edu.hk).

Jiangnan Liu is with the Guangzhou Power Supply Bureau of Guangdong Power Grid Co., Ltd, Guangzhou 510620, China (e-mail: xjy7641@sina.com).

Binghao Li, is with the CSG Electric Power Research Institute, China Southern Power Grid, Huangpu 510663, China (e-mail: tommylbh@foxmail.com).

Chenguo Yao is with the State Key Laboratory of Power Transmission Equipment and System Security and New Technology, Chongqing University, Chongqing 400044, China (e-mail: yaochenguo@cqu.edu.cn).

Zhongyong Zhao is with the College of Engineering and Technology, Southwest University, Chongqing 400716, China (e-mail: zhaozy1988@swu.edu.cn).

I. Introduction

POWER transformers are critical components within the power system, playing an essential role in power transmission, conversion, and voltage regulation [1]–[3]. Their ability to manipulate voltage and current mitigates fluctuations that degrade power quality or cause equipment failure, enhancing the stability of the overall power system. Consequently, given the critical and costly nature of transformers, their malfunctions not only incur substantial maintenance expenses but also significantly compromise the reliability and economic efficiency of the power system [4], [5]. Therefore, ensuring the reliable operation of power transformers is important for maintaining the safe and stable functioning of the power system [6].

Winding deformation is a common fault in power transformers, often resulting from short-circuit (SC) currents that generate substantial electromagnetic forces. These forces can cause irreversible deformation of the transformer windings. As reported by the International Council on Large Electric Systems (CIGRE), winding deformation accounts for approximately 30% of transformer faults. In practice, assessing winding conditions requires draining the transformer oil for internal visual inspection, which is time-consuming and low-efficiency. To overcome these difficulties, researchers have developed various diagnostic methods using various measured signals, including short circuit impedance (SCI) [7], low voltage impulse (LVI) [8], frequency response analysis (FRA) [9]–[11], etc. Among these, FRA has gained the most popularity among researchers and related maintenance personnel as an effective technique for detecting winding deformation because of its precision, simplicity, cost-effectiveness, efficacy, and non-destructive nature. FRA is an offline diagnostic technique used to detect transformer winding faults through graphical analysis, which is currently a widely adopted method in periodic inspection of transformer windings, phase by phase [2], [3]. Specifically, FRA employs the frequency response fingerprint, also referred to as the transfer function or FRA data, to interpret winding deformation faults.

The frequency response fingerprint of transformer windings can be determined through both direct measurement and simulation using equivalent circuit models. In simulations, these models are developed to investigate the influence of various physical deformations on the winding's frequency response fingerprint, offering a more efficient and cost-effective approach compared to destructive physical experiments. Consequently, an accurate equivalent circuit model facilitates cost-free simulations of transformer winding faults [9], [11] and enables the generation of data for data-driven fault diagnosis methods [1], [12], [13]. Furthermore, the interpretation of frequency response fingerprints for winding fault diagnosis currently relies heavily on expert experience, which means that an accurate winding model can help maintenance personnel improve the objectivity of their judgments.

Currently, there are three common methods for establishing FRA-based winding equivalent circuit models:

1) Black-box models use multiple RLC units to simulate resonance points in their frequency response fingerprints, without requiring details of the physical structure of the transformer [14], [15]. While yielding similar frequency response fingerprints, this approach provides information lacking physical significance, rendering it unsuitable for investigating the influence of transformer winding faults.
2) White-box models, usually constructed via finite element method (FEM) based on the transformer's physical structure and material properties, directly derive the frequency response fingerprints from the electromagnetic field [9], [11]. However, this approach is computationally intensive and time-consuming, but it often yields simulated data that deviates significantly from measured data.
3) Grey-box models are a variant of the black-box models, which first construct an equivalent circuit using prior physical knowledge and then identify parameters through optimization algorithms, such as genetic algorithm (GA) and particle swarm optimization (PSO), based on measured frequency response fingerprints [16]–[20]. However, this parameter identification process frequently necessitates extensive adjustments to the search parameter space to obtain optimal parameters that yield a close match with the measured data.

Therefore, this study proposes a two-step broadband equivalent circuit modeling method for transformer windings based on FRA and Bayesian optimization (BO) to address the drawbacks mentioned above. The main contributions are as follows:

1) We propose a two-step broadband equivalent circuit modeling method for transformer windings, offering a generalizable approach applicable to other transformers. The proposed model, implemented in Simulink, simulates the frequency response of both healthy and faulty transformer windings while retaining physical significance.
2) Unlike previous studies that employed an unrestricted parameter space, we use a white-box model to generate a set of feasible parameter solutions, which serve as a reference for subsequent parameter identification. This approach substantially increases both the probability and speed of obtaining viable solutions.
3) In contrast to previous studies employing conventional optimization algorithms with mean squared error (MSE) as a fitness function, we adopt a sample-efficient multi-objective Bayesian algorithm (MOBO), utilizing three common fitness functions as distinct optimization objectives. BO-based algorithms reduce computational costs by minimizing the number of model executions required for parameter identification.

The remainder of this study is organized as follows: Section II introduces the methodology, Section III presents the results, Section IV presents the discussion and limitations, and Section V provides the conclusions.

II. Methodology

A. Basic principle of FRA and proposed model

Under high-frequency excitation, typically above 1 kHz, the transformer core exhibits negligible excitation effects, allowing the winding to be represented as a passive linear two-port network characterized by distributed parameters, including resistors, inductors, and capacitors [17]. In practice, sinusoidal signals $\vec{R}_{in}(\omega)$ with frequencies ranging from 1 kHz to 1 MHz are applied to the input terminal of the winding, and the corresponding response signals $\vec{R}_{out}(\omega)$ are measured at the output terminal, yielding the frequency response fingerprint $T(\omega)$, as defined in Equation (1). The condition of the winding, whether healthy or faulty, is characterized by this frequency response fingerprint. Specifically, the distributed parameters are influenced by the geometric dimensions of the winding. Therefore, any winding deformation alters these parameters, which causes shifts in the resonance points, thereby changing the frequency response fingerprint. By comparing the measured FRA data with a baseline (healthy) fingerprint, maintenance personnel can analyze these variations to assess the condition of the winding [2], [3].

$$T(\omega) = 20\log_{10}\left|\frac{\vec{R}_{\text{out}}(\omega)}{\vec{R}_{\text{in}}(\omega)}\right| \text{dB} \tag{1}$$

where $\vec{R}_{\text{in}}(\omega)$ and $\vec{R}_{\text{out}}(\omega)$ are excitation and response signals, and $T(\omega)$ is the frequency response fingerprint (amplitude versus frequency). According to existing FRA standards [21]–[23] and Refs. [2], [3], this study uses a frequency range of 1 to 1000 kHz.

The ladder network model is a widely adopted approach for modeling transformer windings [16], [17], [24]. This model represents the winding as cascaded equivalent units, each comprising passive circuit elements (i.e., R, G, L, and C) and corresponding to a single- or multi-disk winding. Due to the typically uniform structure of the transformer winding, a complete winding can be effectively modeled as a cascade of these repeatedly connected equivalent units. As shown in Fig. 1, L represents the self-inductance of the winding, R represents resistance (i.e., copper loss), C_s characterizes the inter-disk capacitance effect, G_s characterizes the inter-disk leakage current loss, C_g represents the capacitance between a

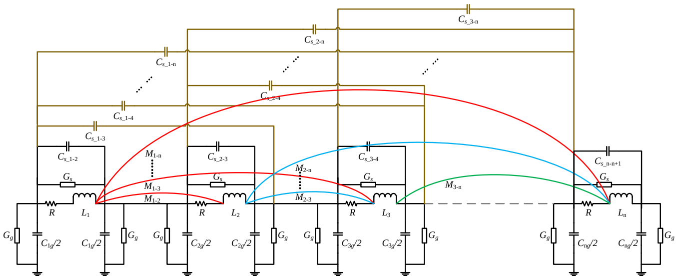

Fig. 1. The proposed equivalent circuit model of transformer winding, considering long-distance mutual inductances and capacitances.

winding disk and ground, G_g represents the ground leakage current loss, and M represents the mutual inductance between different disks.

At low frequencies, transformer windings exhibit predominantly inductive characteristics, whereas at high frequencies, they display predominantly capacitive characteristics [17]. Regarding the former, substantial mutual inductance persists even between distantly separated disks, owing to the coaxial arrangement of the windings. For the latter, whereas most prior studies overlooked the long-distance capacitance, this study incorporates it to simulate high-frequency FRA characteristics as accurately as possible. Besides, it should be noted that the proposed model is specific to the high-voltage winding phase and does not account for coupling effects between the high- and low-voltage windings or among the different phases. The exclusion of the low-voltage winding is a consequence of the ladder network model simplification detailed in Ref. [24]. Furthermore, the omission of inter-phase coupling is justified by the limited influence on FRA data obtained from the single-phase measurement with other windings open-circuited [16], [24], [25].

B. Basic principle of Bayesian optimization

This study necessitates parameter identification for the model depicted in Fig. 1. It is important to note that the parameters within each equivalent unit are not identical, resulting in a high-dimensional parameter space. Previous methods often simplified this by copying parameters from a single unit across all others, thereby reducing the search parameter space [18]. However, this approach introduces inaccuracies given the inherent variations among individual winding disks. Furthermore, conventional intelligent algorithms, such as GA and PSO, are unsuitable for such high-dimensional parameter identification problems, particularly when interacting many times with a complex model. Specifically, these conventional methods require millions of model executions during the optimization process, placing excessive demands on computational resources [26]. Therefore, to address this parameter search challenge and minimize model executions, this study combines BO with specially designed objective functions to obtain an optimal set of circuit parameter values.

BO employs a Gaussian process (GP) to construct a posterior probability distribution by iteratively combining existing observations with their corresponding objective function evaluations. An acquisition function is then used to intelligently guide the selection of the subsequent observation most likely to yield the global optimum. Fig. 2 provides an illustrative example of single-objective BO to find the minimum of a given function.

C. Details of Two-step modeling

This study proposes a two-step modeling method for transformer winding, with the complete procedure detailed in Algorithm 1:

1) Step 1: A three-dimensional (3D) model of the transformer is constructed in ANSYS Maxwell, incorporating its physical structure and material properties, including insulation oil, pressboard, spacers, tank, and core. Subsequently, FEM is used to determine the values of the circuit parameters, as shown in Fig. 1, with detailed calculations presented in the following section.

2) Step 2: An equivalent circuit model is constructed in Simulink. Subsequently, a parameter search space is defined, encompassing the range ±5% around the parameter values derived in Step 1. Then, MOBO is employed for parameter identification [27], guided by three specifically designed objective functions, as delineated by Equations (2)-(5). To be specific, Ob_1 quantifies the overall fitting accuracy, Ob_2 evaluates the similarity between the measured and simulated FRA data [17], and Ob_3 is designed to optimize the fitting of resonance points, whose accuracy is closely related to the accuracy of subsequent fault simulations [2], [18]. In addition, the sparse axis-aligned subspace (SAAS) GP [28] is utilized in conjunction with the parallel noise expected hypervolume improvement (qNEHVI) as the acquisition function for MOBO, representing a state-of-the-art (SOTA) approach for high-dimensional optimization problems [26].

$$Ob_1 = \sum_{i=1}^{N} \left(\frac{T_{actual}\left(w_i\right) - T_{model}\left(w_i\right)}{T_{actual}\left(w_i\right)} \right)^2 \tag{2}$$

$$\begin{aligned} Ob_2 = &\sum_{i=1}^{N} \left(\frac{T_{actual}(w_i) - T_{model}(w_i)}{T_{actual}(w_i)} \right)^2 + \\ &\beta \left(\frac{\sum_{i=1}^{N} \left(T^*_{actual}(w_i) T^*_{model}(w_i)\right)}{\sqrt{\sum_{w=1}^{N} \left(T^*_{model}(w_i)\right)^2 \sum_{w=1}^{N} \left(T^*_{actual}(w_i)\right)^2}} + 1 \right)^{-1} \end{aligned} \tag{3}$$

$$T^*(w_i) = |T(w_i)| - \frac{1}{N} \sum_{i=1}^{N} |T(w_i)| \tag{4}$$

$$Ob_3 = \sum_{i_{RP}=1}^{N_{RP}} \left(\frac{T_{actual}\left(w_{i_{RP}}\right) - T_{model}\left(w_{i_{RP}}\right)}{T_{actual}\left(w_{i_{RP}}\right)} \right)^2 \tag{5}$$

where T_{actual} and T_{model} are actually measured and model-simulated FRA data, respectively. N is the number of measured and simulated sample points, N_{RP} is the number of measured and simulated resonance points, and β represents a hyperparameter, which is assigned a value of 5 in this study.

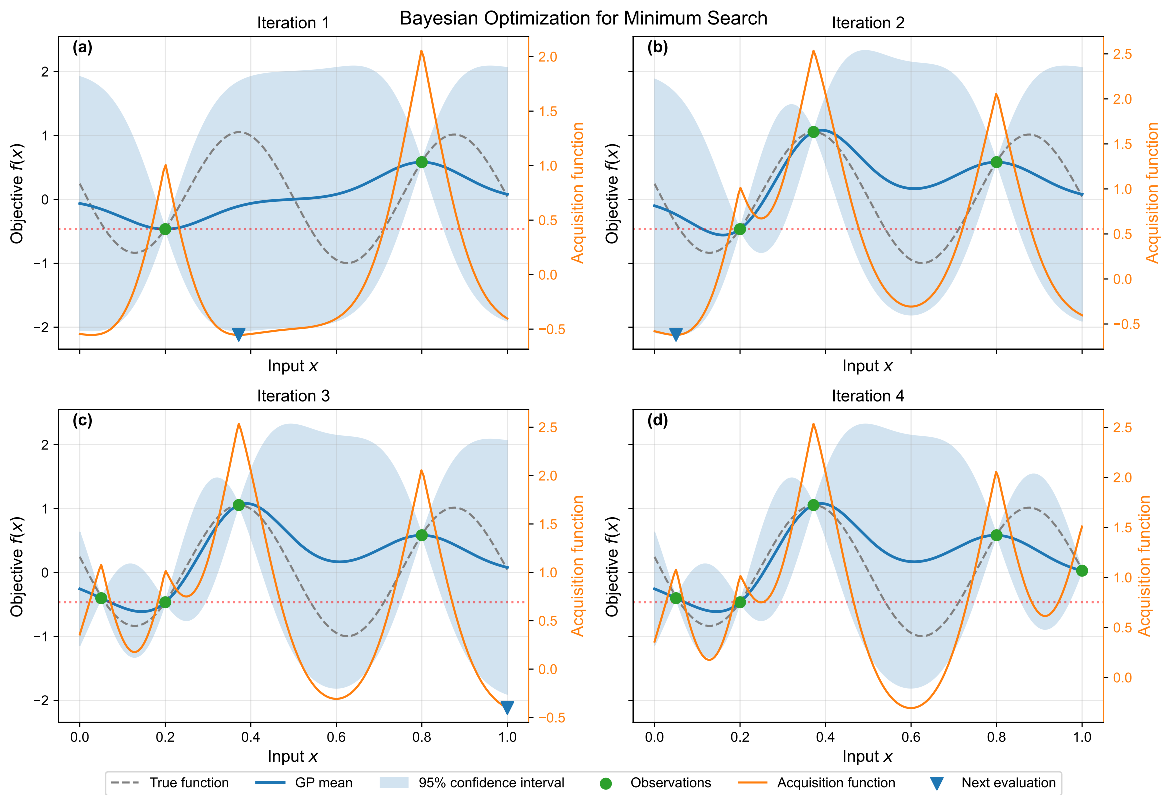

Fig. 2. Illustration of the Bayesian optimization process to find the minimum of a simple function. A Gaussian process model predicts the function values (solid blue line) along with associated uncertainties (blue shading) based on previously collected data. Subsequently, an acquisition function leverages this model to evaluate the potential ”value” of future measurements, thereby balancing exploration and exploitation. The next observation is then selected by minimizing the acquisition function in the parameter space. This iterative process continues until the optimization objectives are achieved.

TABLE I
DIMENSIONAL PARAMETERS OF THE EXPERIMENTAL TRANSFORMER

Parameter		Value	
Iron core diameter (mm)		300	
Iron core yoke length (mm)		1390	
Iron core yoke height (mm)		1190	
Turn to turn spacing (mm)		3	
Disk to disk separation (mm)		2 (1-10, 21-30 disks, and 11-20 disks bottom) and 26 (11-20 disks top)	
Tank (mm)		1705 × 740 × 1415	
Number of disks		30	
Number of turns per disk		10	
Number of parallel		1	
High voltage winding		Low voltage winding	
Inner radius (mm)	421	Inner radius (mm)	316
Outer radius (mm)	500	Outer radius (mm)	349
Height (mm)	520	Height (mm)	87.5

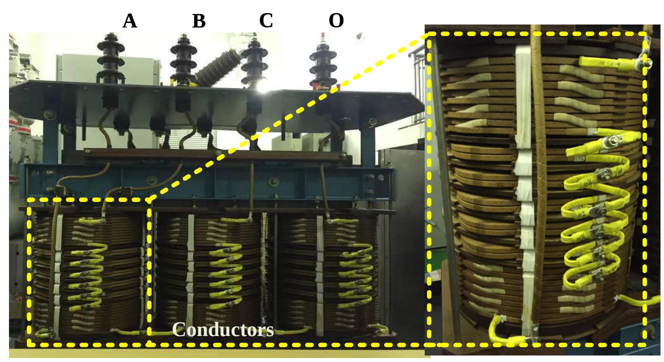

Fig. 3. Internal structure of the specially designed 10 kV transformer.

III. EXPERIMENT RESULTS

A. Experiment settings

The experimental subject is a specially designed 10 kV power transformer, as shown in Fig. 3. Detailed design parameters for this transformer are provided in Table I. Internally, the transformer is structured according to the design principles of the conventional 110 kV transformer. It features a core-type construction, with the high-voltage winding configured as a disc-type winding comprising a total of 30 disks. The top and bottom sections each consist of 10 disks wound in an interleaved pattern, while the middle section encompasses 5 sets of double-disk continuous windings. The low-voltage winding is designed as a layer-type winding, composed of 6 layers. Specifically, this study focuses on the A-phase of the high-voltage winding, thereby building a model with 30 equivalent units.

A 3D transformer model is constructed in ANSYS Maxwell based on physical designs, including considerations for insulation materials (such as insulation oil, pressboard, and spacers) as well as the properties of the tank and core, cross-sectional geometry, number of turns, and coil diameter. The built model is illustrated in Fig. 4, and properties of insulation material within the transformer are shown in Table. II. The calculation

Algorithm 1 Two-step modeling method for the transformer winding.

Input: Objectives $f_{obj} = (Ob_1(x), Ob_2(x), Ob_3(x))$; initial evaluation budget $m \geq 2$; total evaluation budget $T > m$; data storage set H; initial observation set $x_{1:m}$, and evaluations $y_{1:m}$ (optional). // x and y are vector values that contain multiple parameters (i.e., values of circuit parameters) and objectives, respectively.

Output: Based on evaluations, manually choose the best observation x_{best}, y_{best} in the Pareto-optimal set. If the model-based FRA data are not very matched, constrain the search space to ±5% around x_{best} and iterate steps 3-10.

1: A transformer model is constructed using ANSYS Maxwell.
2: The circuit parameters are determined using the FEM.
3: Set the calculated parameters in Step 1 within ±5% as the bounded search space X, $x \in$X.
4: If $x_{1:m}$, $y_{1:m}$ is not provided, let x_t be a Sobol sequence and let $y_t = f_{obj}(x_t)$, $x_t \in$ X, for $t = 1, ..., m$. // Construct the initial observation set and get evaluations.
5: **For** $t = m+1, \ldots, T$ **do**
6: Let $H_t = \{x_{1:t-1}, y_{1:t-1}\}$.
7: Use H_t to fit SAAS GP.
8: Use QNEHVI to obtain the next observation x_t.
9: Evaluate $y_t = f_{obj}(x_t)$. // Input the observation into the built model to obtain an evaluation.
10: **end**
11: **return** Pareto-optimal set $\{x_{1:a}, y_{1:a}\}$.

of these equivalent relative dielectric parameters can refer to Ref. [25].

TABLE II
PROPERTIES OF INSULATING MATERIALS WITHIN THE TRANSFORMER.

Material	Relative dielectric constant
Pressboard	4.7
Insulation oil	2.2
Insulating cylinder/ring	4.5
Spacers	4.7

For capacitance calculation, the transformer tank and iron core are assigned a zero potential. Each disk is assigned a distinct potential, and then the capacitances between the 30 disks, as well as the ground capacitance of each disk, are subsequently computed. Similarly, the inter-disk capacitances are calculated using ANSYS electrostatic field analysis, while the equivalent longitudinal capacitance is determined based on the principle of electric field energy conservation. Specifically, in each field simulation, for an n-conductor system, n independent simulations are automatically performed. The energy stored in the electric field due to the capacitance between any two conductors is then given by [11], [25]:

$$W_{ij} = \frac{1}{2}\int_{\Omega} D_i \times E_j d\Omega \tag{6}$$

where W_{ij} represents the energy stored in the electric field due to flux lines connecting charges on conductor i to those on conductor j, D_i denotes the electric flux density associated

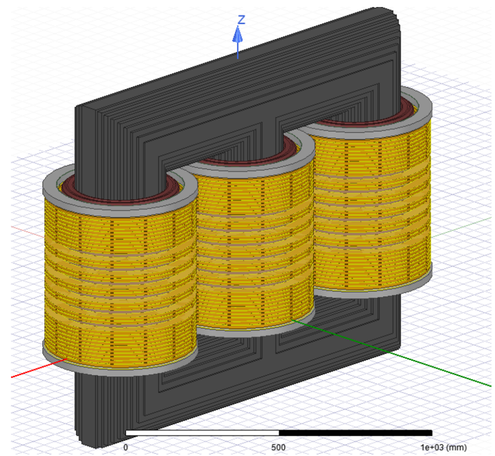

Fig. 4. 3D finite element model of transformer. This study focuses exclusively on the computed inductance, capacitance, and resistance parameters for the high-voltage A-phase winding due to the limited influence from other windings and computational resource restrictions.

with conductor i, and E_j represents the electric field associated with conductor j. Therefore, the capacitance between the conductors i and j is:

$$C_{ij} = \frac{2W_{ij}}{V_{ij}^2} \tag{7}$$

where V_{ij} denotes the electric potential between the conductors i and j. Related results are presented in Fig. 5. It should be noted that, as illustrated in Table I, the increased axial distance between the 10th to 20th winding disks directly leads to a reduction in their calculated capacitance values compared to other winding disks.

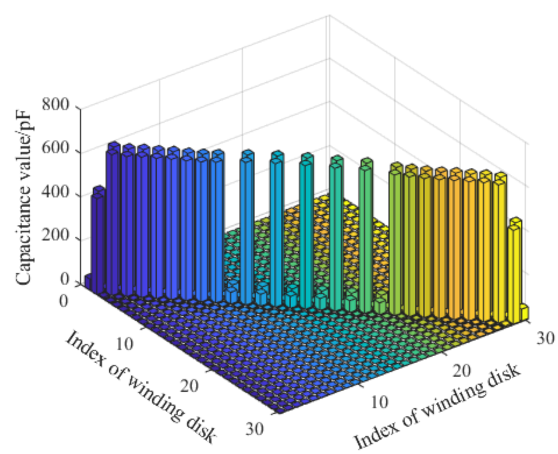

Fig. 5. Capacitance value between different disks.

For the determination of inductance parameters, a current excitation is applied to each winding disk, and the self-inductances and mutual inductances between the 30 disks are then computed. The primary motivation for constructing the circuit model is to accurately represent the transformer winding's frequency response. Given that the frequency range of interest for FRA is above 1 kHz, where the influence of the transformer core is negligible, it is necessary to remove

This article has been accepted for publication in IEEE Transactions on Dielectrics and Electrical Insulation. This is the author's version which has not been fully edited and content may change prior to final publication. Citation information: DOI 10.1109/TDEI.2025.3635100

the iron core from the model when calculating inductance parameters [9], [11]. Specifically, to calculate the inductance, the average magnetic energy, W_{AV}, should be first calculated as [11], [25]:

$$W_{AV} = \frac{1}{4} \int_V B \times H dV \tag{8}$$

where B is the magnetic flux density, H is the magnetic field strength, and V is the volume of the conductor. Then, the inductance can be calculated from the average magnetic energy:

$$L = \frac{4W_{AV}}{I_{Peak}^2} \tag{9}$$

where I_{peak} is the peak winding current. Related results are depicted in Fig. 6.

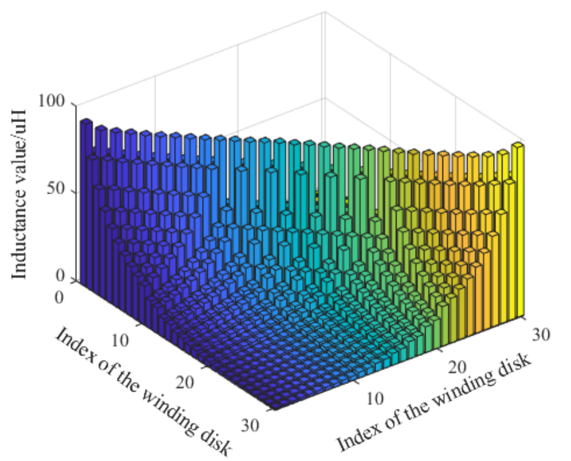

Fig. 6. Self-inductance and mutual inductance of different disks.

Within a fundamental unit of a ladder network, the resistance characterizes the inherent resistance of a single disk. While this parameter can be determined by formula-based calculation $R = \rho\frac{l}{S}$, the resistance obtained via this method represents the direct current (DC) resistance. This value assumes a uniform current density distribution within the winding under a constant DC current, and thus does not account for the skin effect or the proximity effect. To enhance the accuracy of resistance calculation, this study establishes a two-dimensional finite element model of two adjacent winding disks within the ANSYS Maxwell eddy current field. This model is based on the physical dimensions. A defined current excitation is applied to obtain the current density distribution within each turn, as illustrated in Fig. 7. Due to the proximity effect, a symmetrical current density distribution is observed. The currents within the turns exhibit mutual repulsion, effectively displacing the moving charges in adjacent conductors towards their edges. When considering each turn as a whole, the current density distribution also displays a skin effect, concentrated along the surface of the conductor. The computed resistance parameters for each turn are presented in Fig. 8, with turns numbered 1 to 20 from left to right and top to bottom. As can be observed, the middle turns (5th, 6th, 15th, and 16th turns) exhibit higher resistance values, while the end turns (1st, 10th, 11th, and 20th turns) demonstrate slightly lower resistance values. There is a discernible difference in resistance between the end and middle sections, with a calculated value of 15.46 $m\Omega$ at the end and 16.76 $m\Omega$ in the middle. The average resistance is 16.3695 $m\Omega$ in one equivalent unit.

For the determination of electric conductance, which characterizes leakage current losses, it is important to note that each turn is wrapped in insulation paper and the entire winding is immersed in transformer insulation oil. Consequently, the resulting leakage current is typically negligible. According to Refs. [9], [11], [16], [17], the electric conductance is generally on the order of $M\Omega$. Therefore, in this study, an electric conductance value of 10 $M\Omega$ is adopted, and this parameter is not included in Step 2.

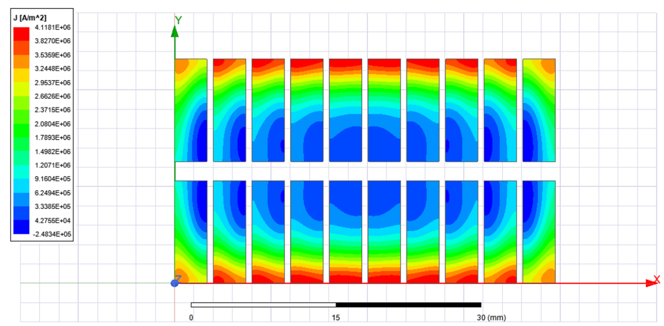

Fig. 7. Current density distribution within each turn under the influence of proximity effect.

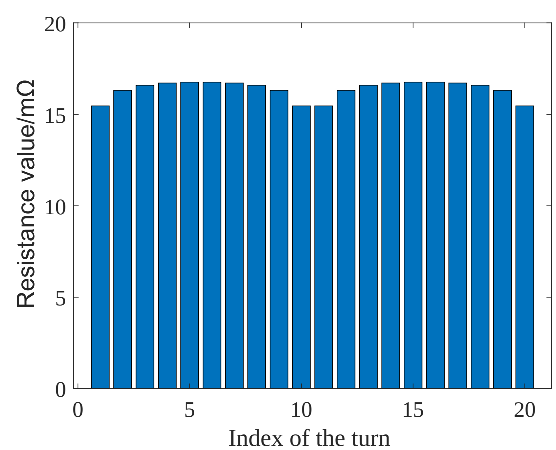

Fig. 8. Equivalent resistance parameters of two adjacent winding disks (total 20 turns).

It should be noted that conventional modeling approaches typically assume circuit parameters to be frequency-invariant. However, parameters such as resistance and inductance, excluding capacitance, manifest frequency-dependent characteristics under varying excitation frequencies. Given the absence of geometric modifications to the winding structure throughout the simulation process, the mutual inductance coefficients between different winding disks are presumed to remain constant. Accordingly, the self-inductance parameters of a representative winding disk are computed across a range of frequencies, thereby yielding the scaling coefficients (i.e., $\eta_{\text{frequency}} =$

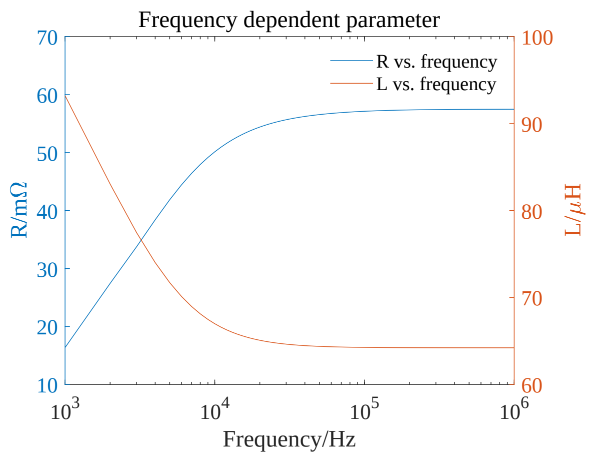

Fig. 9. Frequency-dependent characteristics of the resistance and inductance for a representative winding disk.

$L_{\text{frequency}}/L_{\text{baseline}}$). These coefficients are subsequently applied to the inductance matrix via scalar multiplication, facilitating the generation of frequency-specific inductance matrices. An analogous methodology is employed for resistance parameters. Fig. 9 shows the frequency-dependent characteristics of both resistance and inductance for a representative winding disk. The results presented in Figs. 6-8 are based on computations performed at 1 kHz. Thus, to derive L (including M) and R values at varying frequencies, the 1 kHz baseline values are scaled by the calculated coefficients $\eta_{\text{frequency}}$, as depicted in Fig. 9. Fundamentally, the proposed method entails calculating a single set of circuit parameters at 1 kHz, with adjustments for other frequencies achieved through multiplication by the calculated scaling coefficients $\eta_{\text{frequency}}$.

B. Comparative experiments

The equivalent circuit model depicted in Fig. 1 is constructed in Simulink. Subsequently, the frequency response fingerprint of the high-voltage A-phase winding is measured using a frequency response analyzer (model: TDT6U) [1], and the experimental diagram is illustrated in Fig. 10. Following the acquisition of the measured frequency response fingerprint, these data are used in conjunction with the built model to formulate the three objective functions described in Section 2.3. These objective functions are then minimized through an iterative optimization process that involves the interaction between the Simulink model and the MOBO implemented in Python. The optimized results are presented in Fig. 11. Furthermore, Fig. 11 includes single-step modeling results.

From Fig. 11, it can be seen that: (1) A significant discrepancy exists between the measured and the simulated FRA data derived solely from Step 1. This discrepancy arises due to the idealized nature of the FEM and its lack of direct interaction with measured data. (2) While utilizing only Step 2 (i.e., employing optimization algorithms to identify circuit model parameters) can yield acceptable results, it is important to acknowledge that these results are obtained through iterative MOBO. The computational time required for this approach is approximately 30 times greater than that of the proposed two-step method. (3) The two-step modeling method uses

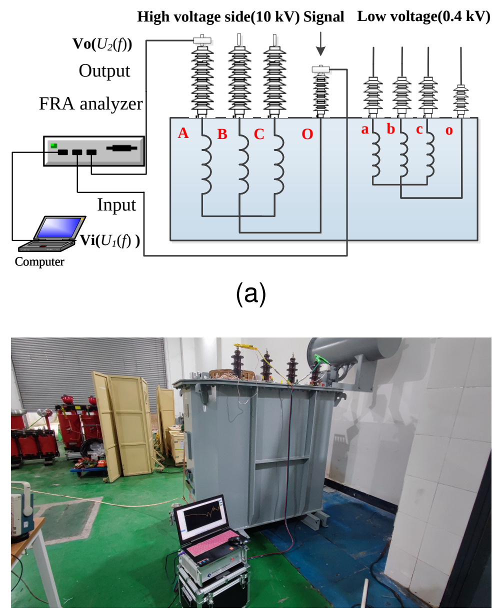

(a)

(b)

Fig. 10. Measurement experimental diagram. (a) Measurement wiring diagram. (b) Actual wiring diagram.

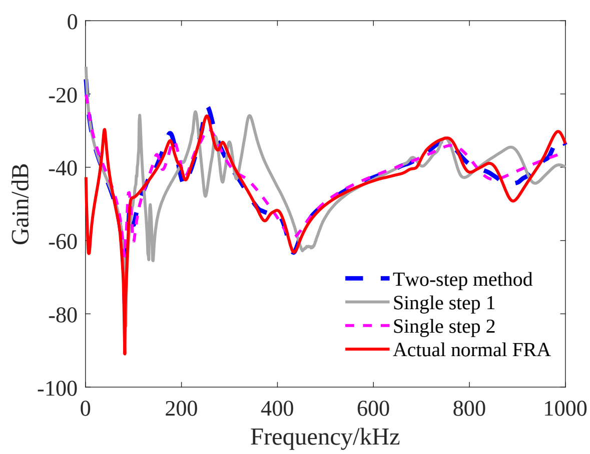

Fig. 11. Results of the two-step and single-step modeling about the normal winding. Single step 1 and Single step 2 essentially represent modeling transformer windings using white-box and gray-box models, respectively. This study focuses on model-based winding fault simulation. Black-box models are excluded from consideration due to their inherent inability to simulate winding faults.

the results of the first step as a reference for setting the initial parameter search space in Step 2, followed by fine-tuning parameters through the minimization of the objective functions. The former action constrains the search parameter space, while the latter enhances the correlation between the measured and simulated data. However, it should be noted that in comparison to the measured FRA data, the simulated one does not capture the first resonance point, likely due to the exclusion of the iron core's influence in the modeling process. In the low-frequency range, despite the frequencies reaching the kilohertz range, the excitation effect of the iron core is not entirely negligible.

This study presents results for different modeling approaches regarding the normal winding, as illustrated in

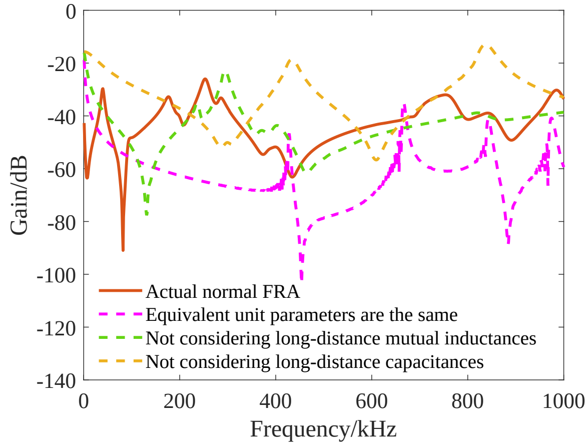

Fig. 12. Results of different models about the normal winding.

Fig. 12. The incorporation of long-distance mutual inductance and capacitance, along with the use of distinct parameter values for each unit, proves beneficial for establishing an accurate equivalent circuit model.

C. DSVs and IDSC simulation based on the built model

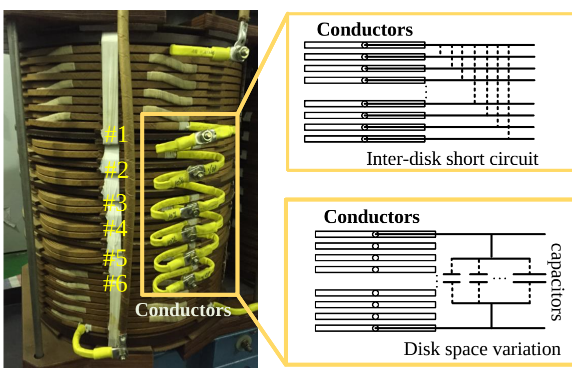

Fig. 13. Simulation wiring diagram for DSVs and IDSCs.

To further validate the accuracy of the proposed model, this study compares the simulated winding fault FRA data with the corresponding measured FRA data, encompassing inter-disk short circuits (IDSCs) and disk space variations (DSVs).

Regarding IDSCs, experimental validation can be performed by directly short-circuiting the conductors, as illustrated in Fig. 13. Different fault locations are achieved by varying the pairs of short-circuited conductors [1]. For instance, IDSC-#1-#2 denotes an IDSC between conductors #1 and #2. In the built model, such IDSC faults are simulated by short-circuiting the equivalent units associated with the corresponding disks. A comparison between the simulated and measured FRA data is presented in Fig. 14.

DSVs are characterized by a reduction in the inter-disk spacing, which predominantly manifests as an increase in inter-disk capacitance within the equivalent circuit model. This alteration is equivalent to introducing parallel capacitors between adjacent disks [1], thereby providing an alternative current pathway through the winding and perturbing the distribution of the winding's leakage magnetic field, as depicted in Fig. 13. For instance, DSV-#1-#2-57pF denotes a DSV between conductors #1 and #2 achieved via the insertion of a 57 pF parallel capacitor. In the built model, DSVs are simulated by incorporating a capacitor between the corresponding units. A comparison between the simulated and measured FRA data is provided in Fig. 15.

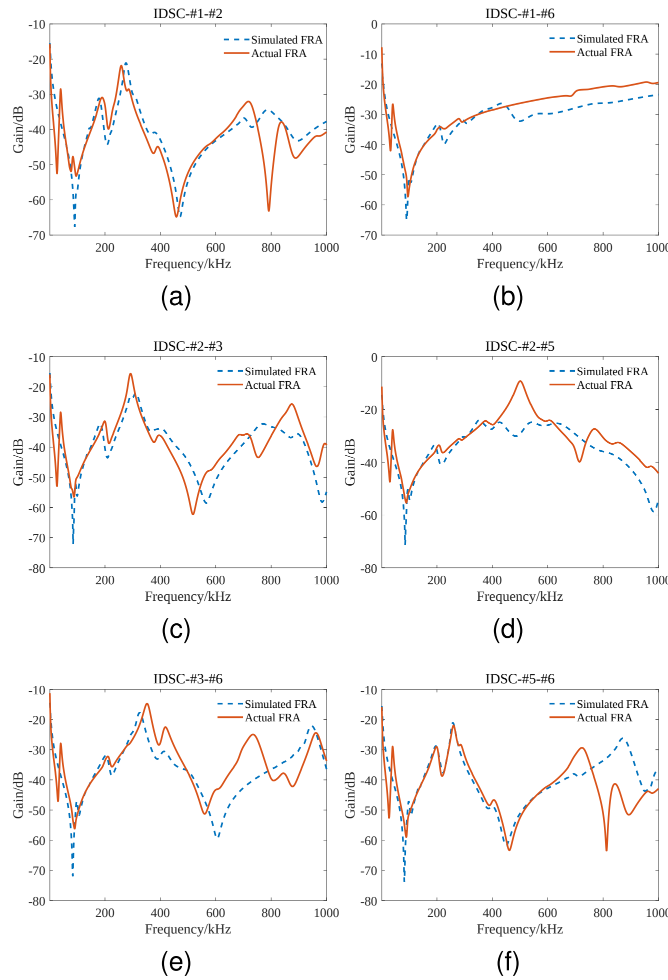

Fig. 14. Several FRA data of IDSCs obtained from actual measurement and model-based simulation. (a). IDSC-#1-#2. (b) IDSC-#1-#6. (c). IDSC-#2-#3. (d). IDSC-#2-#5. (e). IDSC-#3-#6. (f). IDSC-#5-#6.

As observed in Figs. 14 and 15, the simulated IDSCs and DSVs, derived from the built model, exhibit a reasonable degree of consistency with actual measurements within the frequency ranges of 1–600 kHz and 1–900 kHz, respectively. This agreement further supports the practical applicability of the proposed model. However, the consistency is diminished in the high-frequency range, which may be attributed to an incomplete representation of stray capacitance. Furthermore, numerous studies, as evidenced by Refs. [16], [29], [30], have demonstrated that resonance points within the low- and mid-frequency ranges contain the most fault information. The model exhibits small deviations from the measured fault signatures in the low- and mid-frequency ranges. Consequently, it provides a valuable reference for decision-making in practical fault detection.

It should be noted that the simulation results presented in

This article has been accepted for publication in IEEE Transactions on Dielectrics and Electrical Insulation. This is the author's version which has not been fully edited and content may change prior to final publication. Citation information: DOI 10.1109/TDEI.2025.3635100

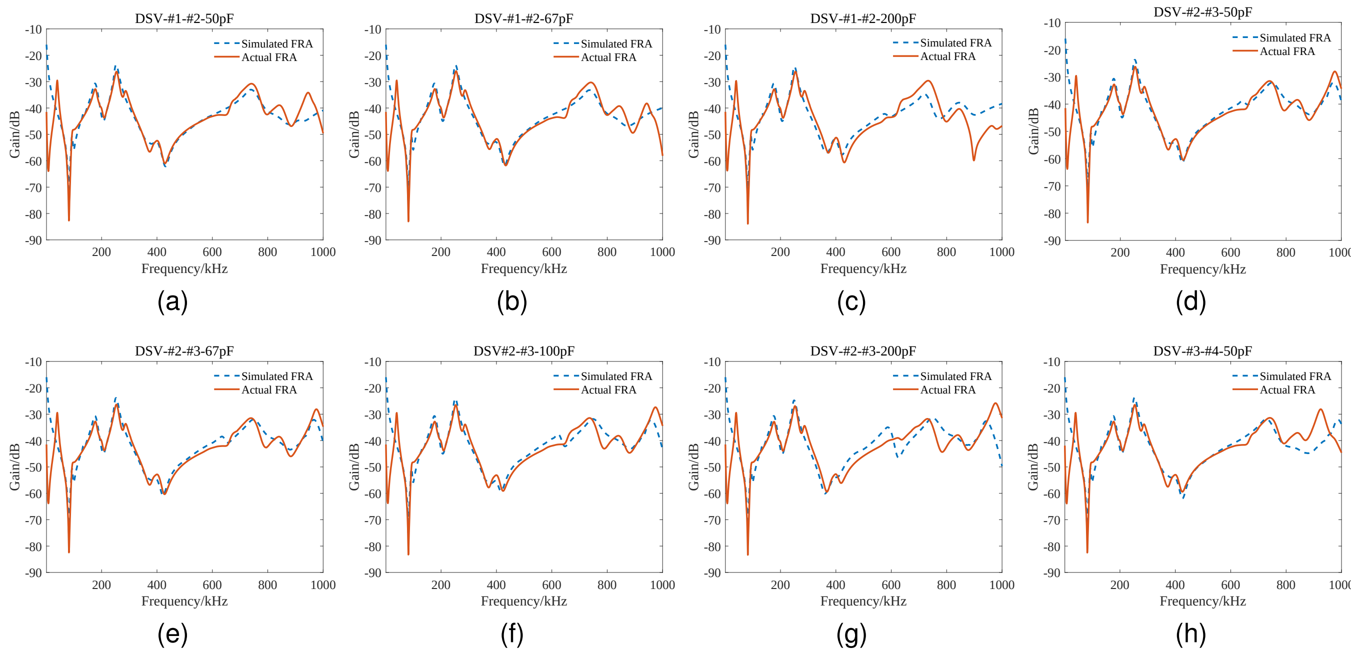

Fig. 15. Several FRA data of DSVs obtained from actual measurement and model-based simulation. (a). DSV-#1-#2-50pF. (b). DSV-#1-#2-67pF. (c). DSV-#1-#2-200pF. (d). DSV-#2-#3-50pF. (e). DSV-#2-#3-67pF. (f).DSV-#2-#3-100pF. (g). DSV-#2-#3-200pF. (h). DSV-#3-#4-50pF.

Figs. 14 and 15 are based on the model built in the previous section, where only short circuits or parallel capacitors are introduced, leaving the circuit parameters unmodified.

IV. Discussion and Limitation

Currently, numerous studies have investigated transformer winding modeling using three types of models: black-box, white-box, and gray-box models. In contrast to black-box models [14], [15], the proposed model incorporates physical interpretations. Indeed, the proposed method combines the advantages of both white-box and gray-box models, leveraging the former to reduce the computational burden associated with parameter space exploration and the latter to mitigate the discrepancy between measured and simulated frequency response fingerprints. Compared to previous studies on white-box models [9], [11], [25], the proposed method demonstrates closer agreement between the simulated and measured FRA data under normal and faulty conditions. Furthermore, the identified parameters exhibit greater physical significance than those obtained by directly applying optimization algorithms to a gray-box model with an unrestricted parameter space [16]–[20].

During the transformer periodic inspections, FRA remains the predominant diagnostic method. However, its accuracy is often constrained by the subjective expertise of maintenance personnel [2]. The built model could address this limitation by providing an objective interpretive framework, such as elucidating FRA data across diverse fault types and locations [9], [11]. Besides, while data-driven methods leverage FRA data to develop intelligent fault diagnosis models [13], their robustness is limited by the paucity of practical fault data [1]. By exploiting physical simulations within the built model, synthetic datasets can be generated to augment the training dataset, thereby fostering a synergistic integration of physical models and data-driven methods that enhance generalization and predictive accuracy.

While the proposed method demonstrates advantages in terms of model performance and physical interpretability, it still has several limitations:

1) This study focuses solely on the A-phase of the high-voltage winding and does not account for the coupling between the high- and low-voltage windings, nor the coupling between the three phases. This is attributed to the limited influence of these coupling effects on the measured single-phase FRA data. Furthermore, the computational complexity and associated time requirements pose a significant challenge in the development of a complete FEM model that considers these coupling effects. However, given that conventional offline FRA for winding fault diagnosis is typically performed phase by phase, the single-winding model developed in this study offers practical applicability.
2) The scope of winding faults simulated in this study is limited. It is difficult to use circuit-based models to emulate various mechanical faults due to the difficulty in quantifying the associated circuit parameters for certain complex deformations or components, such as radial deformation or bushing conditions [31], [32].

V. Conclusion

This study proposes a two-step broadband equivalent circuit modeling method for power transformer winding based on FRA and BO. Based on the experimental and comparative results, the following conclusions are drawn:

1) The proposed model, which employs distinct parameter values for each unit and incorporates long-distance mu-

This article has been accepted for publication in IEEE Transactions on Dielectrics and Electrical Insulation. This is the author's version which has not been fully edited and content may change prior to final publication. Citation information: DOI 10.1109/TDEI.2025.3635100

tual inductance and capacitance, demonstrates superior agreement with measured FRA data from a physical transformer.

2) To address the challenges associated with high-dimensional parameter identification, this study employs FEM to derive an initial parameter set in Step 1. This precalculation significantly reduces the computational time required for subsequent fine-tuning of circuit parameters using optimization algorithms based on measured FRA data in Step 2. Furthermore, this method facilitates data interaction between the measured data and the built model, improving the possibility of searching for a set of feasible solutions.
3) To validate the model's performance, several common winding mechanical faults are simulated. The simulated FRA changing trends exhibit strong agreement with the measured data, thereby indirectly confirming a robust mapping relationship between the model and the actual transformer. Furthermore, simulated FRA data can serve as a valuable reference for subsequent fault diagnosis.

REFERENCES

[1] Y. Chen, Z. Zhao, J. Liu, S. Tan, and C. Liu, "Application of generative ai-based data augmentation technique in transformer winding deformation fault diagnosis," *Engineering Failure Analysis*, vol. 159, p. 108115, 2024.

[2] M. H. Samimi and S. Tenbohlen, "Fra interpretation using numerical indices: State-of-the-art," *International Journal of Electrical Power Energy Systems*, vol. 89, pp. 115–125, 2017.

[3] W. C. Sant'Ana, C. P. Salomon, G. Lambert-Torres, L. E. Borges da Silva, E. L. Bonaldi, L. E. de Lacerda de Oliveira, and J. G. Borges da Silva, "A survey on statistical indexes applied on frequency response analysis of electric machinery and a trend based approach for more reliable results," *Electric Power Systems Research*, vol. 137, pp. 26–33, 2016.

[4] C. Gezegin, O. Ozgonenel, and H. Dirik, "A monitoring method for average winding and hot-spot temperatures of single-phase, oil-immersed transformers," *IEEE Transactions on Power Delivery*, vol. 36, no. 5, pp. 3196–3203, 2021.

[5] T. Manoj, C. Ranga, A. Abu-Siada, and S. S. M. Ghoneim, "Analytic hierarchy processed grey relational fuzzy approach for health assessment of power transformers," *IEEE Transactions on Dielectrics and Electrical Insulation*, vol. 31, no. 3, pp. 1480–1489, 2024.

[6] T. Zhang, L. Li, Y. Wang, N. Zhang, S. Jiang, and A. Abu-Siada, "Analysis of transformer oil-paper insulation state using fractional poynting–thomson model," *IEEE Transactions on Dielectrics and Electrical Insulation*, vol. 29, no. 2, pp. 583–590, 2022.

[7] F. Yang, S. Ji, Y. Liu, and F. Zhang, "Research of sweep frequency impedance to determine transformer winding deformation after short-circuit impact," in *2016 IEEE International Power Modulator and High Voltage Conference (IPMHVC)*, 2016, pp. 68–72.

[8] V. A. Lavrinovich and A. V. Mytnikov, "Development of pulsed method for diagnostics of transformer windings based on short probe impulse," *IEEE Transactions on Dielectrics and Electrical Insulation*, vol. 22, no. 4, pp. 2041–2045, 2015.

[9] N. Hashemnia, A. Abu-Siada, and S. Islam, "Improved power transformer winding fault detection using fra diagnostics – part 1: axial displacement simulation," *IEEE Transactions on Dielectrics and Electrical Insulation*, vol. 22, no. 1, pp. 556–563, 2015.

[10] Y. Akhmetov, V. Nurmanova, M. Bagheri, A. Zollanvari, and G. B. Gharehpetian, "A bootstrapping solution for effective interpretation of transformer winding frequency response," *IEEE Transactions on Instrumentation and Measurement*, vol. 71, pp. 1–11, 2022.

[11] N. Hashemnia, A. Abu-Siada, and S. Islam, "Improved power transformer winding fault detection using fra diagnostics – part 2: radial deformation simulation," *IEEE Transactions on Dielectrics and Electrical Insulation*, vol. 22, no. 1, pp. 564–570, 2015.

[12] A. Moradzadeh, H. Moayyed, B. Mohammadi-Ivatloo, G. B. Gharehpetian, and A. P. Aguiar, "Turn-to-turn short circuit fault localization in transformer winding via image processing and deep learning method," *IEEE Transactions on Industrial Informatics*, vol. 18, no. 7, pp. 4417–4426, 2022.

[13] J. Liu, Z. Zhao, C. Tang, C. Yao, C. Li, and S. Islam, "Classifying transformer winding deformation fault types and degrees using fra based on support vector machine," *IEEE Access*, vol. 7, pp. 112 494–112 504, 2019.

[14] T. A. Papadopoulos, A. I. Chrysochos, A. I. Nousdilis, and G. K. Papagiannis, "Simplified measurement-based black-box modeling of distribution transformers using transfer functions," *Electric Power Systems Research*, vol. 121, pp. 77–88, 2015.

[15] M. F. Horvat, Z. Jurković, B. Jurišić, T. Župan, and B. Ćućić, "Black-box power transformer winding model," in *2022 7th International Advanced Research Workshop on Transformers (ARWtr)*, 2022, pp. 18–23.

[16] F. Ren, H. Zhang, Y. Liu, S. Ji, and Q. Li, "Ladder network synthesis in wide frequency range for transformer winding from its driving-point admittance data," *IEEE Transactions on Power Delivery*, vol. 37, no. 3, pp. 1370–1379, 2022.

[17] R. Aghmasheh, V. Rashtchi, and E. Rahimpour, "Gray box modeling of power transformer windings for transient studies," *IEEE Transactions on Power Delivery*, vol. 32, no. 5, pp. 2350–2359, 2017.

[18] Z. Zhao, Y. Chen, Y. Yu, M. Han, C. Tang, and C. Yao, "Equivalent broadband electrical circuit of synchronous machine winding for frequency response analysis based on gray box model," *IEEE Transactions on Energy Conversion*, vol. 36, no. 4, pp. 3512–3521, 2021.

[19] Y. Chen, X. Ji, and Z. Zhao, "Synchronous machine winding modeling method based on broadband characteristics," *Applied Sciences*, vol. 11, no. 10, 2021.

[20] A. Abu-Siada, M. I. Mosaad, D. Kim, and M. F. El-Naggar, "Estimating power transformer high frequency model parameters using frequency response analysis," *IEEE Transactions on Power Delivery*, vol. 35, no. 3, pp. 1267–1277, 2020.

[21] "Power transformers-part 18: Measurement of frequency response. international standard, iec 60076-18," 2012.

[22] "Ieee guide for the application and interpretation of frequency response analysis for oil-immersed transformers," *IEEE Std C57.149-2012*, pp. 1–72, 2013.

[23] P. Picher, M. Lachman, P. Patel *et al.*, "Advances in the interpretation of transformer frequency response analysis (fra)," *Cigre Technical brochure, Brochure*, vol. 812, 2020.

[24] M. M. Shabestary, A. J. Ghanizadeh, G. B. Gharehpetian, and M. Agha-Mirsalim, "Ladder network parameters determination considering nondominant resonances of the transformer winding," *IEEE Transactions on Power Delivery*, vol. 29, no. 1, pp. 108–117, 2014.

[25] X. Zhao, C. Yao, A. Abu-Siada, and R. Liao, "High frequency electric circuit modeling for transformer frequency response analysis studies," *International Journal of Electrical Power Energy Systems*, vol. 111, pp. 351–368, 2019.

[26] Y. Chen, B. Qin, X. Liu, W. Wang, and Y. Liao, "Start-to-end modeling and transmission efficiency optimization for a cyclotron-based proton therapy beamline," *Nuclear Engineering and Technology*, vol. 56, no. 10, pp. 4365–4374, 2024.

[27] D. Eriksson, P. I.-J. Chuang, S. Daulton, P. Xia, A. Shrivastava, A. Babu, S. Zhao, A. Aly, G. Venkatesh, and M. Balandat, "Latency-aware neural architecture search with multi-objective bayesian optimization," *arXiv preprint arXiv:2106.11890*, 2021.

[28] D. Eriksson and M. Jankowiak, "High-dimensional bayesian optimization with sparse axis-aligned subspaces," in *Uncertainty in Artificial Intelligence*. PMLR, 2021, pp. 493–503.

[29] Y. Chen, Z. Zhao, Y. Yu, W. Wang, and C. Tang, "Understanding ifra for detecting synchronous machine winding short circuit faults based on image classification and smooth grad-cam++," *IEEE Sensors Journal*, vol. 23, no. 3, pp. 2422–2432, 2023.

[30] Z. Zhao, C. Yao, C. Li, and S. Islam, "Detection of power transformer winding deformation using improved fra based on binary morphology and extreme point variation," *IEEE Transactions on Industrial Electronics*, vol. 65, no. 4, pp. 3509–3519, 2018.

[31] Z. Zhao, C. Yao, X. Zhao, N. Hashemnia, and S. Islam, "Impact of capacitive coupling circuit on online impulse frequency response of a power transformer," *IEEE Transactions on Dielectrics and Electrical Insulation*, vol. 23, no. 3, pp. 1285–1293, 2016.

[32] A. Abu-Siada, N. Hashemnia, S. Islam, and M. A. Masoum, "Understanding power transformer frequency response analysis signatures," *IEEE Electrical Insulation Magazine*, vol. 29, no. 3, pp. 48–56, 2013.